Low-angle shear within the exposed Manzalesti salt diapir, Romania: incipient decapitation in the Eastern Carpathians fold-and-thrust belt

Dan M. Tămaş[1], Alexandra Tămaş[2], Jessica Barabasch[3], Mark G. Rowan[4], Zsolt Schléder[5], Csaba Krézsek[6] and Janos L. Urai[3]

[1]Babeș-Bolyai University, Department of Geology, Cluj-Napoca, Romania

[2]Durham University, Department of Earth Sciences, Durham, UK

[3]RWTH Aachen University, Tectonics and Geomechanics, Aachen, Germany

[4]Rowan Consulting, Inc., 850 8th St., Boulder, CO 80302, USA

[5]OMV Exploration & Production GmbH, Vienna, Austria

[6]OMV Petrom S.A., Exploration B.U., Bucharest, Romania

Key points

- the Mânzălești salt diapir evolved from a salt-cored anticline into a thrusted diapir in front of the Tarcău nappe
- foreland-directed movement of the nappe sheared the top of the diapir, leading to incipient decapitation the Mânzălești salt diapir
- the deformation we see in the outcrop happened at a shallow depth and fast strain rates

ABSTRACT

In salt-detached fold-and-thrust belts, contractional modification of diapirs may include decapitation by thrusting, but examples are not well known in the subsurface and unreported in outcrop. Here we present a surface exposure of an intrasalt, sub-horizontal shear zone at the boundary between the Tarcău and Subcarpathian nappes in the Romanian Eastern

Carpathians. The Mânzălești diapir forms the largest rock salt outcrop in Europe, with unique salt-karst geomorphology. Numerous wells show that the outcrop is above deep-seated salt of an original salt-cored anticline whose base is at >3500 m. Multiscale observations using UAV-based digital outcrop models, fieldwork, and microstructure analysis show that the outcrop is characterised by sub-horizontal foliation with isoclinal folds, unlike the subvertical fabric of most Romanian diapirs. The halite is rich in clastic inclusions, with a power-law size distribution caused by tectonic reworking of originally dirty salt. Microstructures show that the halite matrix is strongly deformed by dislocation creep, forming subgrains and dynamically recrystallized grains around large porphyroclasts with piezometry indicating a relatively high differential stress around 4 MPa. The observations are best explained by sub-horizontal shear generated by an overriding nappe, overprinting the original coarse-grained salt fabric during incipient decapitation of the salt diapir at a depth sufficient to supress dilatancy.

Keywords: salt tectonics, fold and thrust belts, sheared diapir, UAV photogrammetry, microstructures

INTRODUCTION

Numerous orogenic fold-and-thrust belts involve salt, with notable examples in Arctic Canada, the Sierra Madre Oriental of Mexico, the Atlas Mts., the Pyrenees, the Alps, the Carpathians, the Zagros Mts., the Salt Ranges of Pakistan, the Kuqa Basin of China, and the Flinders Ranges of Australia (see Davis & Engelder, 1985; Letouzey et al., 1995; Hudec & Jackson, 2007; Duffy et al., 2018 for compilations and further references). In all cases, the salt layer served as an excellent décollement for folds and thrusts (Davis & Engelder, 1985), and in some, diapirs exerted a profound influence on structural styles (e.g., Rowan &

Vendeville, 2006; Callot et al., 2007). Some of these were preexisting passive diapirs that localized contractional strain; others developed only during the shortening. This may happen by salt breaking through the thin roof of an early salt-cored anticline or the thicker roof of a later fold that is thinned erosionally (Coward & Stewart, 1995). Alternatively, salt carried up in the hanging wall of a thrust fault is also a diapir, including when the thrust cuts one or both limbs of a precursor salt-cored anticline (thrusted diapir fold of Mrazec, 1910, or injection fold of Beloussov, 1959).

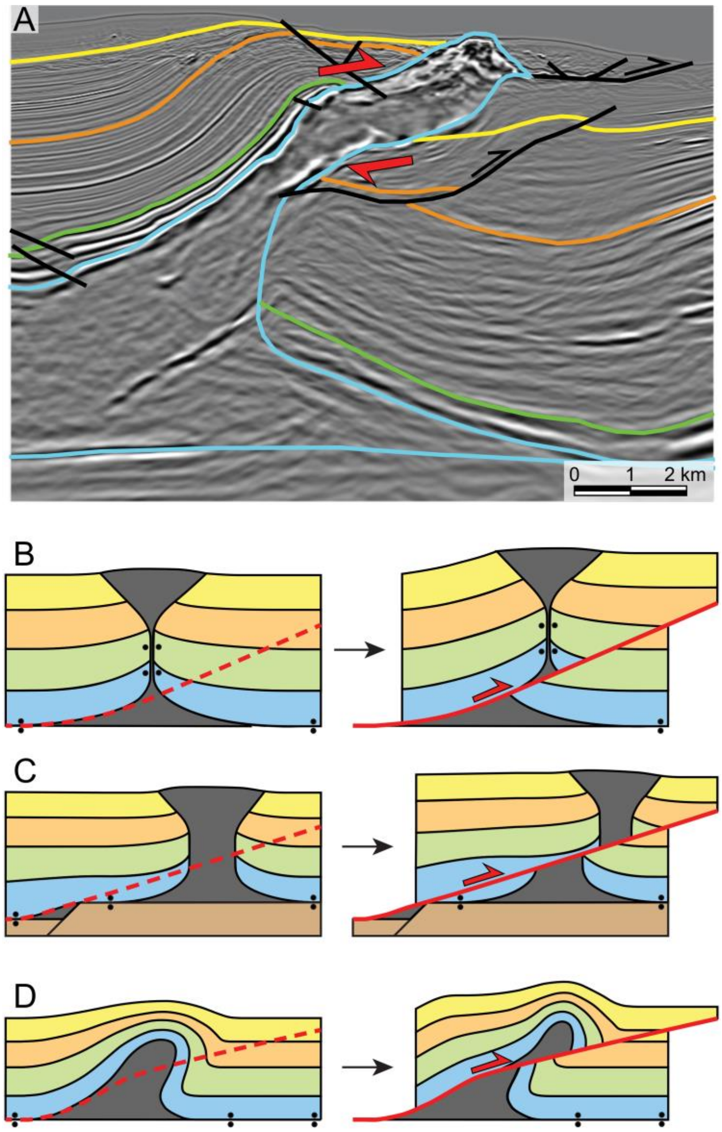

Figure 1. (A) 3-D depth-migrated seismic profile from the Gulf of Mexico (where it is a combined divergent and convergent margin) showing salt diapir (blue) in the process of being decapitated during shortening (no vertical exaggeration, WesternGeco high-quality WAZ

image). (B-D) Schematic diagrams showing different types of diapir decapitation (salt in grey, pairs of dots indicate salt welds): (B) thrust fault emanating from pedestal after formation of vertical weld due to squeezing of diapir; (C) offset of diapir stem and squeezing of upper portion due to thrust fault intersecting diapir above pedestal; (D) salt-cored detachment fold modified by thrust fault, thereby becoming a decapitated diapir.

Whatever the timing and nature of their origin, diapirs are subsequently modified by ongoing contractional deformation. In this setting, diapirs may get decapitated by thrust faults. Indeed, partly or wholly decapitated diapirs have been produced in analogue and numerical models (e.g., Callot et al., 2007; Ferrer, 2012; Pichel et al., 2017; Duffy et al., 2018) and interpreted in the subsurface (e.g., Parravano et al., 2015; Snidero et al., 2019; Fig. 1A). Decapitated diapirs may take several forms. First, after a passive diapir is squeezed shut, forming a secondary salt weld, further shortening leads to a thrust emerging from the diapir pedestal and offsetting the weld from its root (Fig. 1B). Second, decapitation may occur higher on the diapir stem, especially during rift-basin inversion, where thrust faults ramping up over basement steps may intersect diapirs located over the footwalls of the basement faults (Fig. 1C). Third, a thrust fault may break out of a salt-cored detachment fold, thereby generating a diapir (again, thrusted diapir fold or injection fold), shearing the salt, and ultimately translating the upper portion completely off its base (Fig. 1D). In any case, the available subsurface information on decapitated diapirs is patchy at best.

Developing a proper understanding of how diapirs and contractional deformation interact is an important and ongoing research topic for both academia and industry. Despite their being observed in models, interpreted on seismic data, and depicted in cross-sections, decapitated or partially decapitated diapirs have not, to our knowledge, been documented in exposures in orogenic fold-and-thrust belts. Thus, the aim of this paper is to use subsurface data, UAV-based digital outcrop models, outcrop observations and microstructural analysis to demonstrate that the Mânzălești diapir in the Eastern Carpathians of Romania was in the process of being decapitated when shortening-induced shearing ceased and the salt was uplifted to the surface. We anticipate that our findings will spur others, specifically those who are taking a renewed interest in the role of salt in fold-and-thrust belts, to consider the process of diapir decapitation and perhaps identify and analyse further examples.

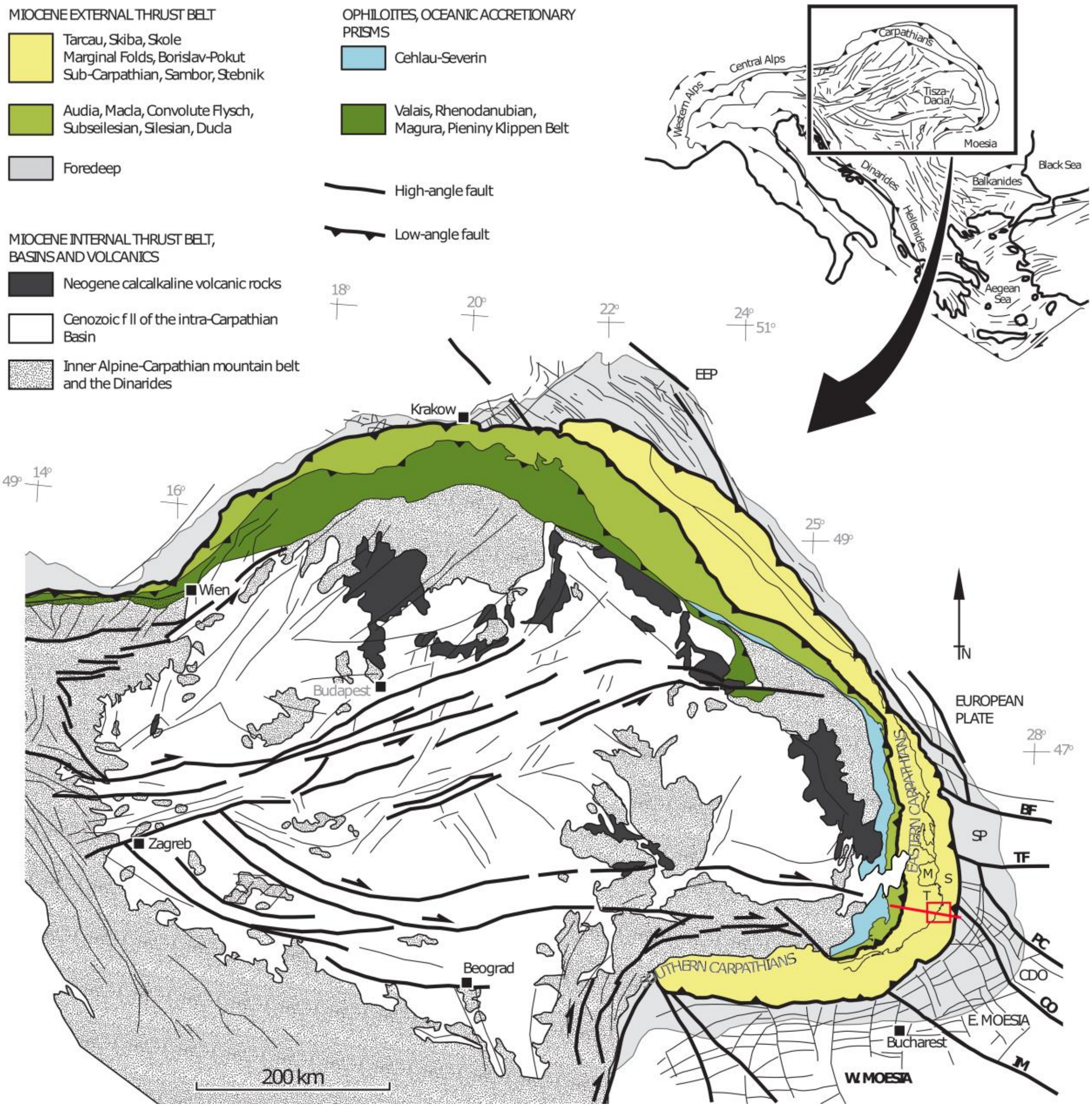

Figure 2. Regional Map of the Alpine - Carpathian - Pannonic orogen, illustrating the major structural features of the Carpathian chain (adapted from Schleder et al., 2019). The Miocene

external nappes in the Romanian Carpathians (yellow on map): T - Tarcău, M - Marginal Folds, and S - Subcarpathian. The inset map illustrates the Alpine - Carpathian belt with its main lineaments. Locations of the surface geological map (Fig. 3A) and regional cross-section (Fig. 3B) are marked with a red polygon and red line, respectively.

GEOLOGIC SETTING

Tectonics and stratigraphy

The study area is located in the south of the Romanian Eastern Carpathians, in the thin-skinned part of this fold and thrust belt (Fig. 2). The Carpathians are an Alpine orogen that records the late Jurassic to middle Miocene closure of the Alpine Tethys (Săndulescu, 1988, 1984; Schmid et al., 2008; Csontos & Vörös, 2004; Maţenco, 2017; Schleder et al., 2019;). The Mânzăleşti diapir (Fig. 3) is one of many salt outcrops located in front of the Tarcău nappe (Dumitrescu, 1948, 1952) and within the Subcarpathian nappe (Mrazec & Voiteşti, 1914; Băncilă, 1958; Fig. 3B). These nappes were emplaced mainly during the middle Miocene contractional event, when the Subcarpathian nappe was thrusted over the undeformed foreland (Săndulescu, 1988, 1984; Maţenco & Bertotti, 2000). The foreland deposits (Fig. 3) are represented by Sarmatian (middle Miocene) to recent clastic sediments deposited in the Dacian Basin (see Lazarev et al., 2020 for more details).

The rocks in the Tarcău nappe are of Mesozoic to middle Miocene age. The stratigraphy in the hanging wall just north and west of the Mânzăleşti salt outcrop is interpreted as lower Miocene in age (Dumitrescu et al., 1970; Stoica & Gherasie, 1981; Maţenco & Bertotti, 2000; Fig. 3). The same lower Miocene age is assigned to the rocks of the Subcarpathian nappe (underneath and exposed south and east of the salt outcrop (Dumitrescu et al., 1970; Stoica and Gherasie, 1981; Maţenco and Bertotti, 2000; Fig. 3B).

The number of salt formations in the Romanian Carpathians and their precise age (lower or middle Miocene) is interpreted differently by different authors (i.e. Cobălcescu, 1883; Athanasiu, 1916; Mrazec & Teisseyre, 1902; Voitești, 1943; Tămaş et al., 2018; Filipescu et al., 2020). However, because the outcome of this discussion is not critical for our interpretation, we use a lower Miocene age for the salt in this paper.

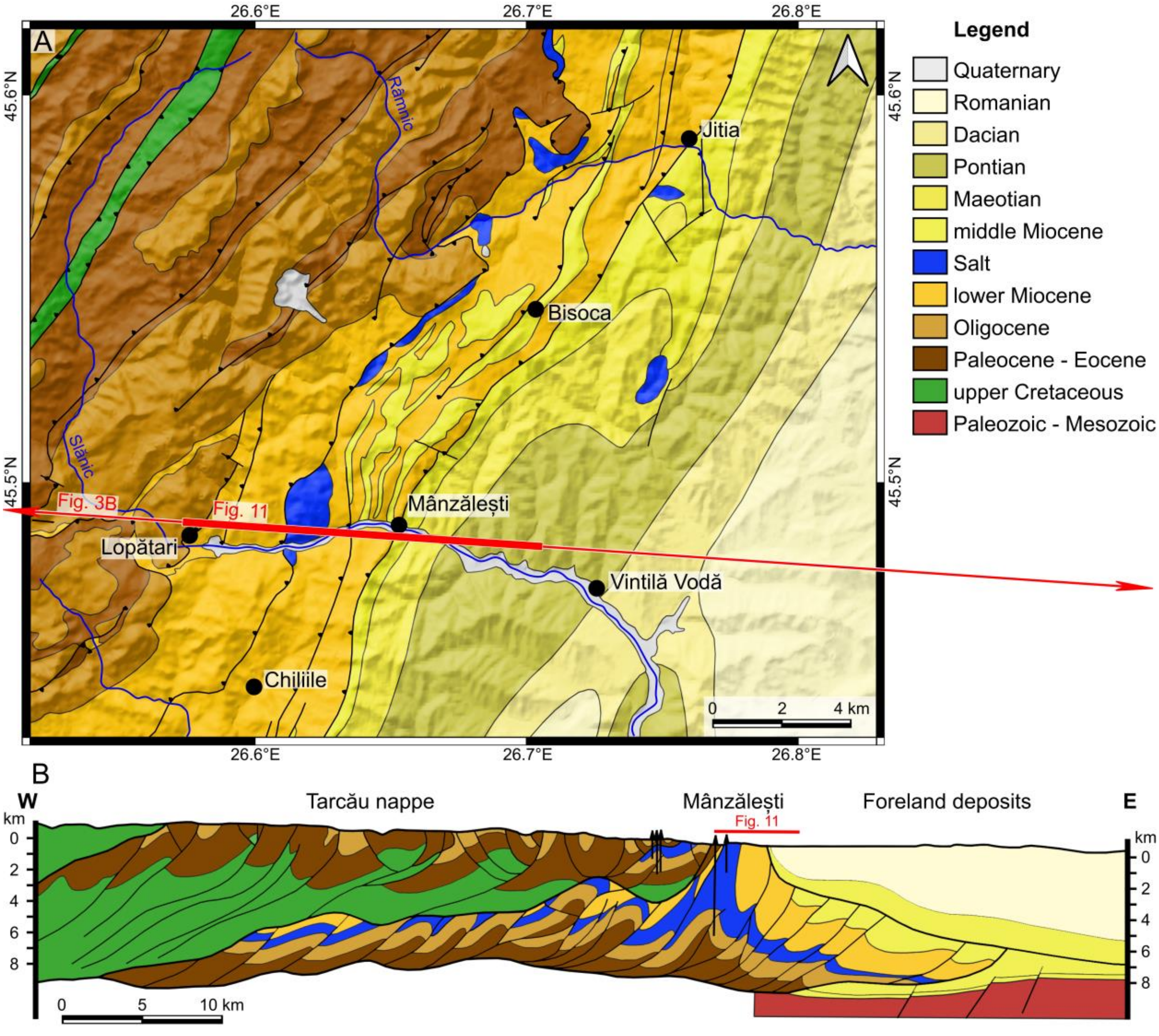

Figure 3. (A) Surface geological map of the study area (Murgeanu et al., 1968) overlain on the EU-DEM v1.1 (grayscale hillshade). The location of section in Figure 3B is marked with a red line on the map, and the location of the section in Figure 11 is highlighted on both the map and regional section. (B) Regional geological profile through the southern part of the

Eastern Carpathians, crossing the Mânzălești salt diapir, derived from surface geology and seismic sections (after Mațenco & Bertotti, 2000).

The Mânzălești diapir

The Mânzălești diapir is located between the villages of Mânzălești, Săreni, Lopătari and Trestioara (Fig. 3A). The top of the salt diapir is known as the Meledic Plateau, which is capped by fluvial Quaternary sediments which, together with the larger inclusions in the salt, form debris flows over the edge of the halite outcrops which are over 35 degrees steep. The area has been the focus of multiple studies related to salt karst formation. This outcrop hosts the 6S cave, which has 3234 m of passages, which is the longest salt cave in Europe and second longest in the world, (Giurgiu, 2010; Melinte-Dobrinescu et al., 2017; Ponta, 2019). The caves within the salt diapir host multiple vegetal and animal remains (i.e. a >12000-year-old molar from an Eqvus hemionus; Giurgiu, 2010). The salt is eroded quite rapidly: it is estimated that the Slănicul de Buzău river carries ~500.000 tons of dissolved halite per year (Stoica & Gherasie, 1981).

The salt is rather impure (82 vol % halite; Stoica & Gherasie, 1981; Giurgiu, 2010), even excluding the very large inclusions (i.e. sandstones, limestones, metamorphics). The origin of the inclusions (tectonic or sedimentary) has long been debated: they have a range of lithologies and could be derived from multiple sources (i.e. the Tarcău or older nappes, Miocene conglomerated in the Tarcău nappe; Stoica & Gherasie, 1981; Meruțiu, 1912; Dumitrescu et al., 1970; Mrazec & Teisseyre, 1902; Popescu, 1951; Olteanu, 1951; Melinte-Dobrinescu et al., 2017).

More than 20 salt and hydrocarbon exploration wells were drilled in the area. They indicate that the base of the salt is at ~3500 m (Meruțiu, 1912; Stoica & Gherasie, 1981; Mațenco & Bertotti, 2000; Fig. 3B).

METHODS AND DATA

In this study we combine well data, satellite images and Digital Elevation Model (DEM) data with Unmanned Aerial Vehicle (UAV) photogrammetry, field observations and microstructural analysis in a multi-scale analysis of internal deformation and structural evolution of the Mânzălești salt diapir.

During recent years, the use of UAV photogrammetry has become a key component of fieldwork in geoscience. Tools for interpreting 3D outcrops in Digital Outcrop Models (DOM) are emerging, and extracting structural data from outcrops that are not easy or safe to reach is now possible. Studies using remote sensing data and UAV methods can much improve observations regarding both geomorphology and deformation (i.e. Jahani et al., 2007; Aftabi et al., 2010; Barnhart & Lohman, 2012; Gutiérrez & Lizaga, 2016; Gutiérrez et al., 2019; Roosta et al., 2019; Weismüller et al., 2019; Bahrami et al., 2020). Field studies in outcrop and in salt mines, combined with microtectonic analysis provide a scale of observation and resolution which complements 3D seismic and drill core data on geometry and and allow microtectonic analysis which provides information on rheology and deviatoric stress (i.e. Talbot & Rogers, 1980; Talbot, 1998; Jahani et al., 2007; Desbois et al., 2010; Schorn & Neubauer, 2014; Závada et al., 2015; Gutiérrez & Lizaga, 2016; Burliga et al., 2018; Sarkarinejad et al., 2018; Zucker et al., 2019).

A vintage seismic line along the Râmnicul Sărat valley and 7 exploration wells (for salt mining and hydrocarbons) were available for this study in the area of the diapir (Meruțiu, 1912; Marica, 2016; Stoica & Gherasie, 1981), providing control on the subsurface structure and stratigraphy. Field measurements and observations were used to complement the interpretation of the subsurface data. Results from analogue modelling experiments aiming to understand deformation in the Eastern Carpathian Bend Zone (Tămaș et al., 2019) provided useful structural analogues in the interpretation of the sub-surface data.

Satellite data

The satellite imagery is publicly available from ESRI. DEM data is from the European Environment Agency under the framework of the Copernicus programme (European Digital Elevation Model, version 1.1 (EU-DEM v1.1), with a pixel size of 25 m and a vertical accuracy of +/- 7 m (land.copernicus.eu).

Unmanned aerial vehicle photogrammetry

In an earlier UAV-based study (Urecheatu et al., 2018), we explored data acquisition and processing for the diapir outcrops. This gave a first indication of the unexpectedly shallow dip of foliation and allowed the selection of optimal parameters for the second-generation data presented in this paper. The UAV photo data were collected using a DJI Mavic Air drone with a 12 MP image sensor. A number of 1725 digital images were acquired for the creation of the DEM and orthorectified image and another 2420 digital images were acquired for the nine detailed DOM.

Before image acquisition, ground control points (GCP) were defined and their locations measured. Manual flight and photograph acquisition were used for the steep faces of the outcrops from altitudes ranging from 50 cm to 150 m (Fig. 4). The photographs of the sediment-covered flat top of the diapir were taken using both manual flight paths and automated flight paths as two orthogonal flight grids. For the automated data acquisition, we used Pix4Dcapture. When flying the manual flight paths, we aimed to achieve a similar photograph overlap as with the automated acquisition.

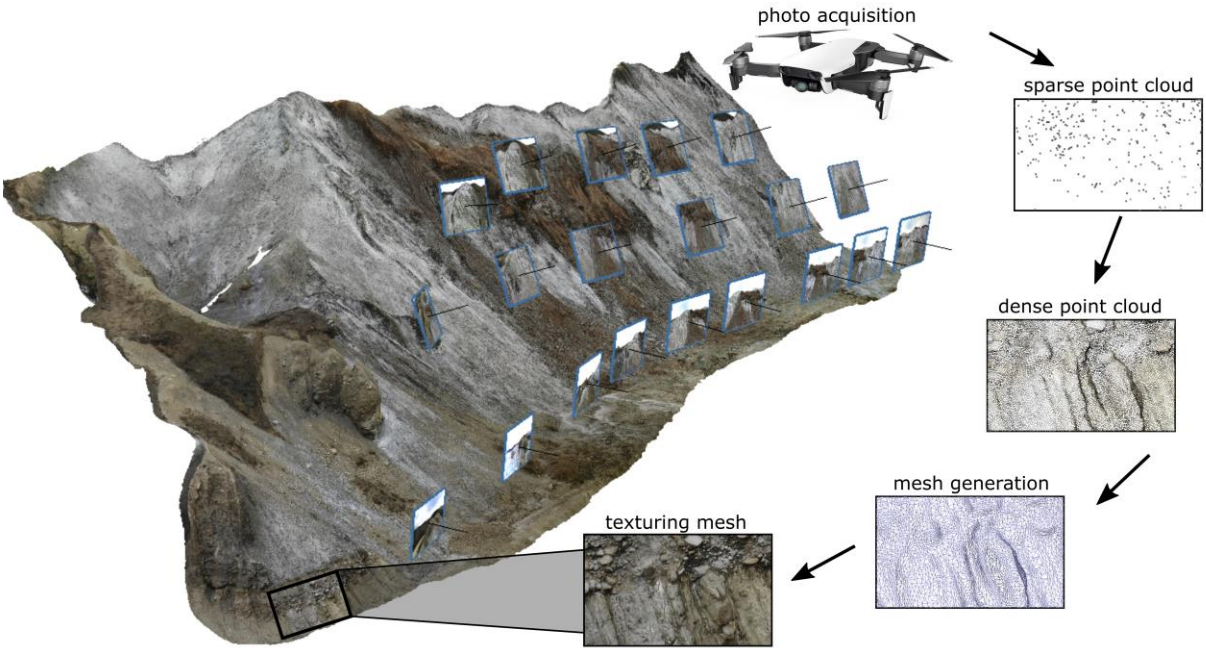

Figure 4. Figure illustrating the main steps used in creating the digital outcrop models in Agisoft Metashape Professional (see Fig. 8 for more details on this model). Note that the photograph thumbnails in the figure are not the real number of images used for the creation of this model.

For the creation of the DOM, DEM and orthorectified models, we used Agisoft Metashape Professional (v.1.6.2). The first step in the process is aligning the photographs, generating a sparse point cloud (Fig. 4). The next step was the generation of the dense point cloud. From the dense point cloud, we then generated both the DEM and the mesh which we later textured (Fig. 4). The position match between the UAV-based orthomosaic and satellite imagery is very good, thus we have a high confidence in the orientation and position of the DOM.

Structural data extraction

The DEM and orthomosaic data were imported in QGIS (QGIS v. 3.14, 2020), which was used to extract boundaries of the salt outcrops, map larger inclusions in the salt, lineations and the size and geometries of the valleys and sinkholes. The 3D textured meshes (DOM) together with the dense point cloud data were imported into Virtual Reality Geological Studio (VRGS v.2.52) software (Hodgetts, 2010) with the scope of interpreting them and extracting the orientation of structural features. We measured the orientation of salt foliation, shear zones and fold axial planes. Orientation data were processed in Stereonet (Allmendinger et al., 2013; Cardozo & Allmendinger, 2013) and Structural Geology to Post Script (SG2PS; Sasvári & Baharev, 2014).

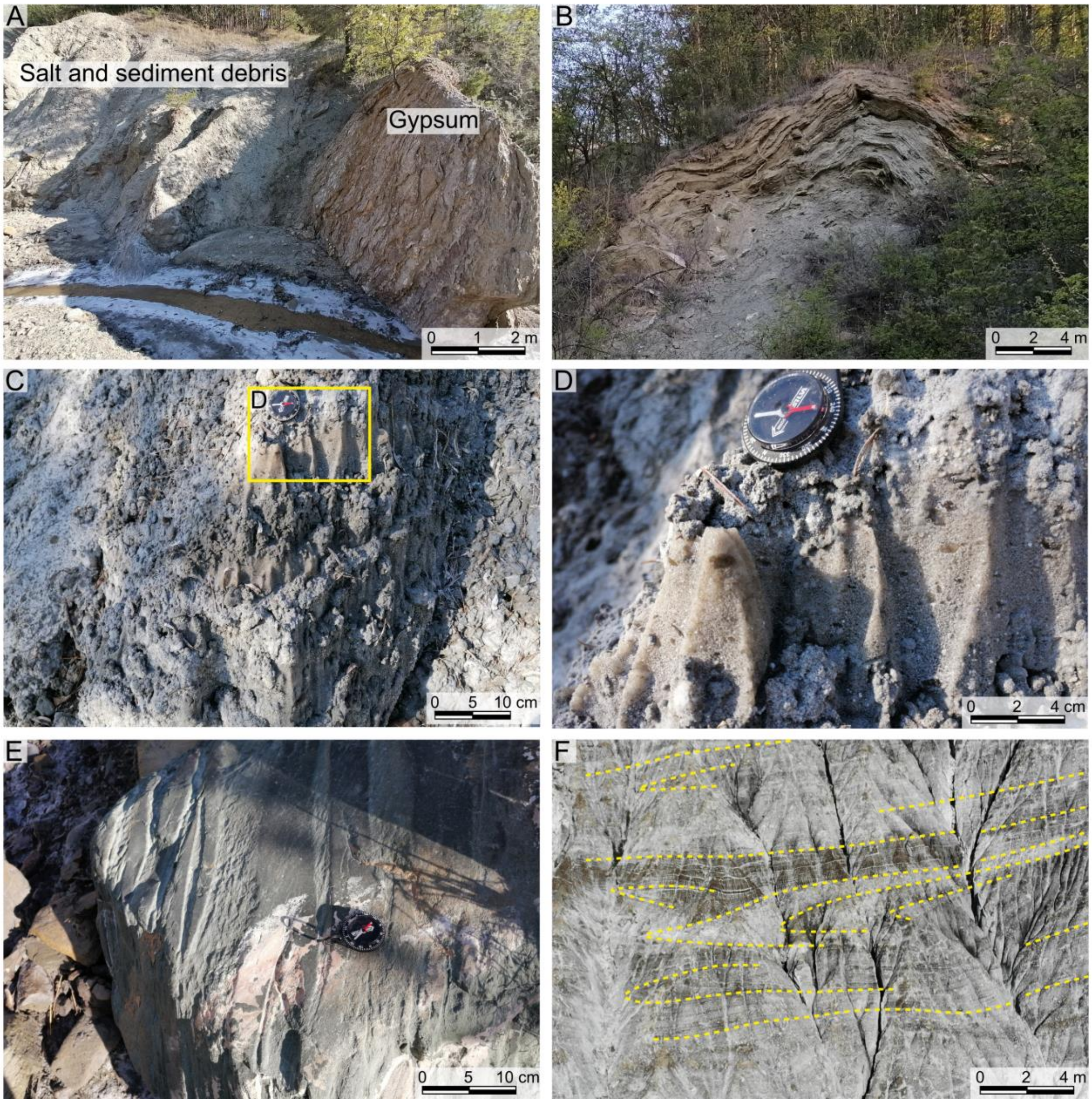

Figure 5. Field photographs. (A, B) Folded gypsum layers on the northern flank of the diapir. (C, D) Salt exposure characterised by rillenkarren (solution grooves) – note the elongated and

euhedral halite grains and large porphyroclasts, and that most of the walls are covered by shale debris and recrystalised salt crusts. (E) Example of dm-scale exotic block – such cm- to m-scale clasts/blocks are found all along the valleys crossing the salt and on the steep outcrops, with the source for these from both the salt and the fluvial deposits on top of the salt diapir being eroded. (F) Drone close-up photograph of salt illustrating isoclinal folding. Figure locations are marked in Fig. 6.

Ground-based field work

Field observations provided information on lithology, orientation of bedding (non-salt units) and foliation in salt and on the structure of salt crusts covering much of the outcrop (Fig. 5). Where accessible, dip and azimuth measurement were taken using both a Freiberg geological compass and FieldMove on an iPad. This helped ground truth the UAV-DOM observations. In addition, samples were taken for microstructural study.

Microstructural analysis

Samples for microstructural analysis were cut in a dry laboratory with a diamond saw cooled by a small amount of slightly undersaturated salt brine to reduce damage. Thin sections were polished to a thickness of approximately 1 mm and then chemically polished and etched using the technique described in Urai et al. (1987). The thin sections were imaged in reflected light using the Petroscan Virtual Petrography system (Spruzeniece et al., 2019). Halite grain and subgrain boundaries were manually traced with a touchpen and tablet and analyzed with Fiji (Schindelin et al. 2012) for subgrain size piezometry (Schleder & Urai 2005). Thereby the grain size was calculated as equivalent circular diameters by only taking halite grains into account. Non-halite inclusions of one hand specimen where peeled onto acrylic foil, scanned and image processed with Fiji (Schindelin et al. 2012). This contributed to an accurate mapping of non-halite inclusions by the utilisation of Fiji image thresholding. For X-ray diffraction (XRD) analysis of inclusions, a hand specimen was dissolved in water and the insoluble residue was hand-picked into three particle classes based on colour (black, beige and greenish). Qualitative and quantitative XRD measurements were then performed on a Bruker D8 equipped with a graphite monochromator and a scintillation counter. Scans were measured with Cu-kα radiation.

RESULTS

Geomorphology

The extent of salt close to the surface is about 2.7 km by 1.3 km, with karstified halite cut by hypersaline streams (Fig. 6). The maximum elevation difference between the lowest point in the riverbed crossing the salt diapir and the highest point of the diapir is 198.5 m. The highest point (613 m) is located in the east-central part of the salt outcrop. Much of the flat top of the salt is covered (Figs. 6-9) by thin quaternary strata and soil, grass, bushes and trees. We focussed our study on steep salt exposures where the salt is usually white to light-grey and the surrounding stratigraphy is pale yellow-brown. Combining our data with geological maps and other published data we estimated the area of salt which is covered by thin quaternary strata (Fig. 6).

The Mânzălești salt diapir has many sinkholes, especially in the south-western area. It is also covered by small lakes, probably associated with sinkholes (i.e. Figs. 6, 8C). The width of the visible sinkholes with salt walls ranges from 7-50 m and their depth from the ridges down to the beginning of the drain is up to 33 m. The drainage system of the Mânzălești salt diapir is localised in several high-order streams cutting through the salt diapir, but not uniformly distributed on its surface (Fig. 6).

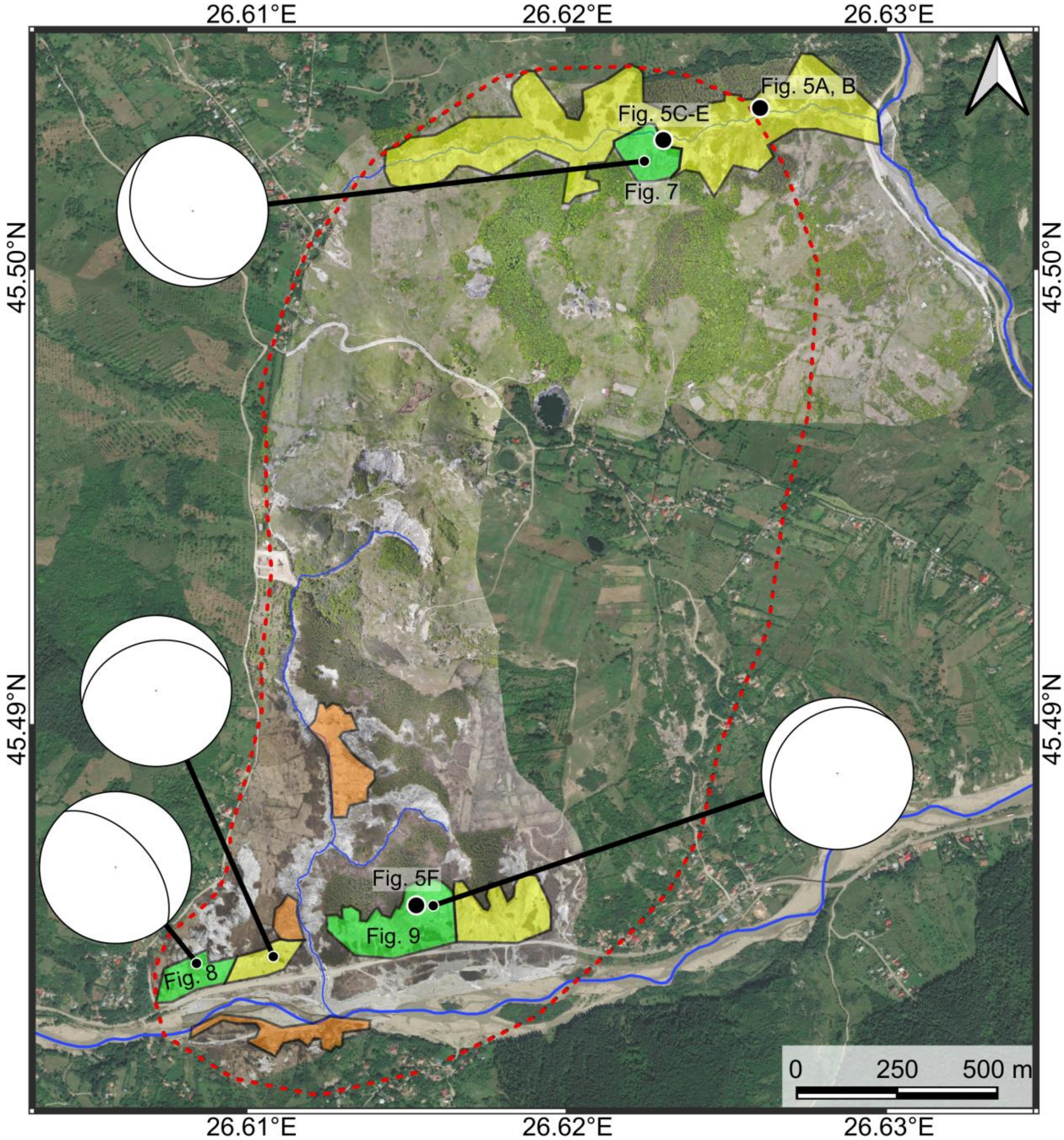

Figure 6. Orthomosaic (light shading) overlaid on ESRI satellite image illustrating streams cutting the diapir (blue lines), the outline of the salt body (red dashed line), salt outcrops (white-light-grey outcrops), and the locations and exposure quality of the detailed DOM (Figs. 7-9). Average salt foliation orientations are shown as great circles on lower-hemisphere stereonets. The models have been classified as good (green), moderate (yellow) or poor (orange) quality based on exposure, amount of debris cover and model-generation quality.

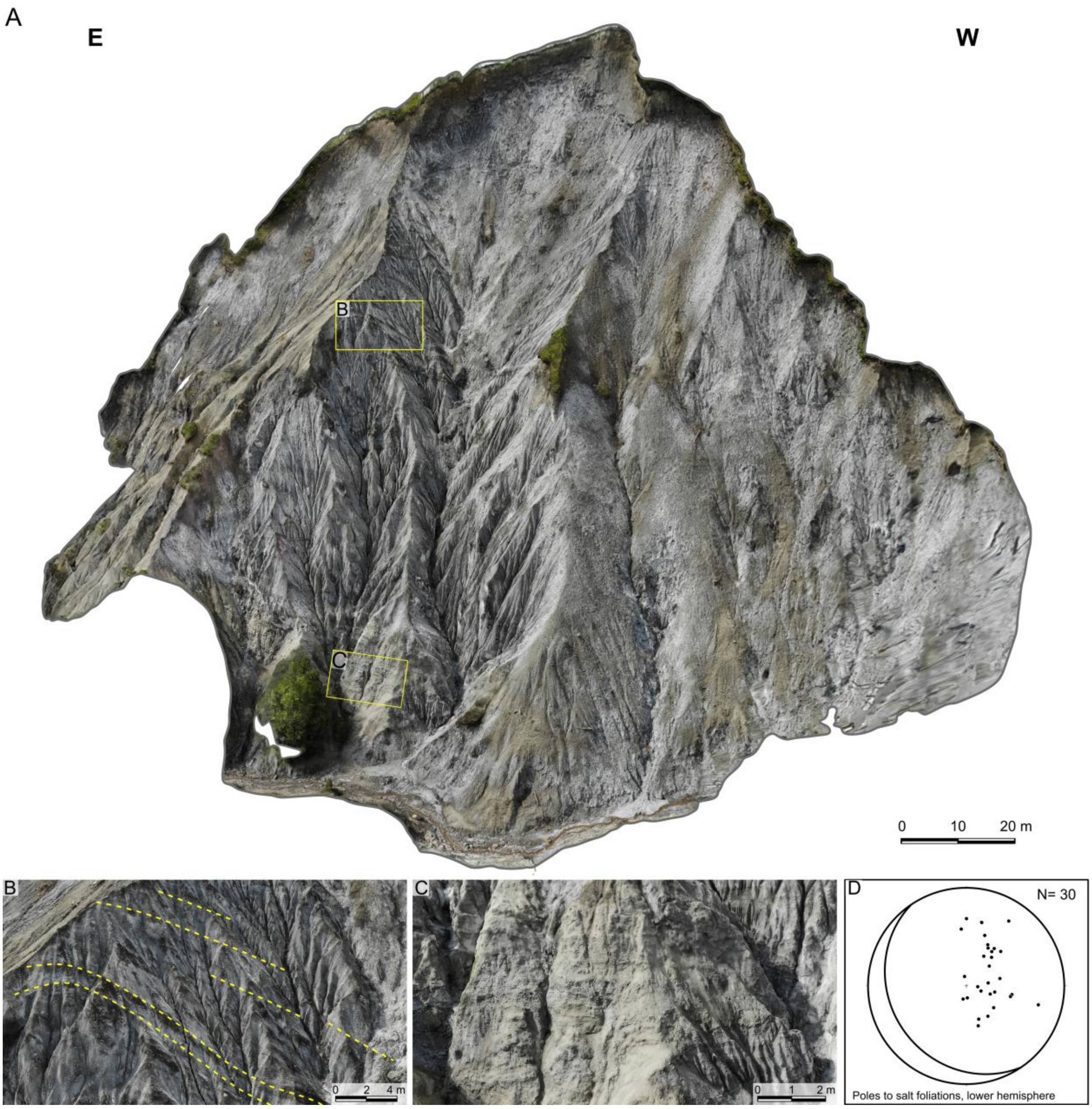

Figure 7. (A) Sideview of DOM 1, located in the NE of the Mânzălești salt diapir (with location of Figs. 7B, C). (B) Detailed image extracted from the DOM illustrating the salt foliation (marked with yellow dashed lines). (C) Detailed image extracted from the DOM illustrating salt interlayered with sandstones. (D) Lower-hemisphere stereonet plot showing poles to foliation) and average orientation as a great circle.

UAV-based models

Four of the nine high-resolution digital outcrop models provided sufficient outcrop quality to allow interpretation and analysis of structures; three of these are described in the paper (Fig. 6). The models with insufficient quality have either too much secondary crusts or debris covering the outcrop and/or locally unsuitable light conditions (Fig. 6).

The models presented expose the foliation and other structures of the salt. Foliation orientation measurements were possible because the deep gullies in the outcrop faces provide two apparent dip measurements (Fig. 6). As will be discussed below, foliation in the salt is generally gently dipping, with some variations between outcrops.

Digital Outcrop Model 1

This DOM (shown in Fig. 7) is located in the northern part of the Mânzălești salt diapir (Fig. 6). This is the only area in the north where salt layering is visible in DOM. The model is 170 m long and 85 m high and has an east-west orientation (Figs. 6, 7). The exposure and model quality are relatively good, with some areas covered by recrystalised salt crusts and debris (Fig. 7). The salt foliation (n = 30) has an average dip of 23° to the SW (Fig. 7D). Sandstone interlayered with the salt are shown in detail in (Fig. 7C).

Digital Outcrop Model 2

The DOM (shown in Fig. 8) is from the south-western edge of the study area, located along the main road between Mânzălești and Lopătari (Fig. 6). The model is 200 m long and 47 m high and has a WSW–ENE orientation (Figs. 6, 8A, C). The exposure and model quality are relatively good, locally covered by recrystallised salt crusts and debris. Several sinkholes can be identified in the model (Fig. 8A, C), ranging from 2-40 m in width and with depths up to 23 m.

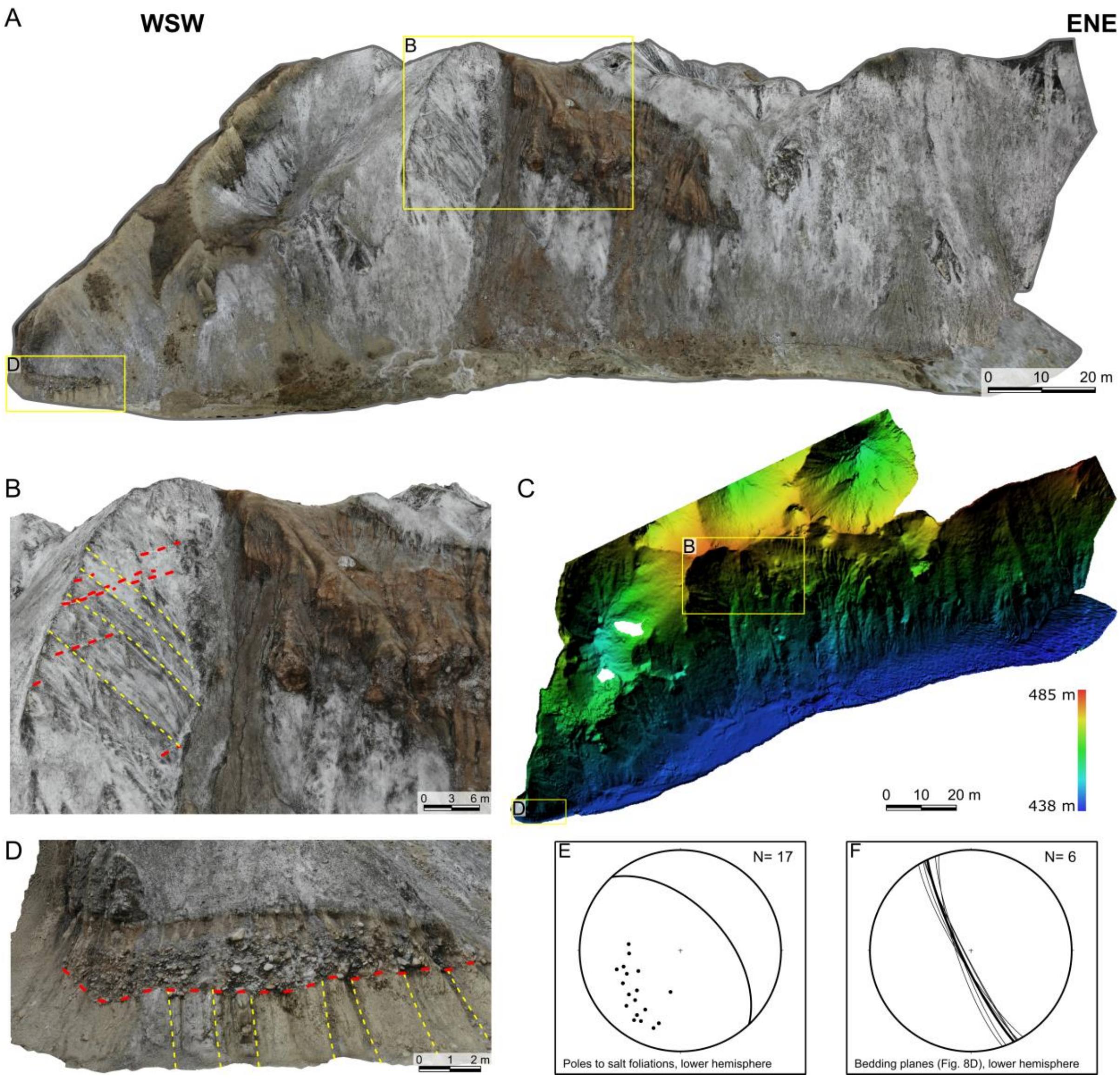

Figure 8. (A) Sideview of DOM 2, located in the SW of the Mânzălești salt diapir (with location of Figs. 8B, C). (B) Detailed image extracted from the DOM illustrating the salt foliation (marked with yellow dashed lines; Fig. 8E) and the white bands cutting the foliation at a low angle (dashed red lines, see also Fig. 9A, B). (C) Digital elevation model (topview) illustrating the large number of sinkholes in the model as well as the location of Figs. 8B, D. (D) Detailed image extracted from the model illustrating the almost vertical bedding (dashed yellow lines) of the lower Miocene stratigraphy flanking the diapir and the discordant (dashed red line) nature of the Quaternary fluvial deposits and the salt on top of these. (E)

Lower-hemisphere stereonet plot showing poles to salt foliation and average orientation as a great circle. (F) Lower-hemisphere stereonet plot showing the bedding planes of the near-vertical lower Miocene strata.

Folds in the salt could not be identified in this outcrop. The salt foliation orientations are the steepest in this area, 53° to the NE (Fig. 9B, E)), locally cross-cut by white, subparallel, low-dipping bands (17° NW; Fig. 8B) whose origin is discussed below. In the western edge of the model, near-vertical (82° WSW; Fig. 8A, D, F) rocks of the Subcarpathian nappe are exposed and truncated by fluvial Quaternary sediments (Fig. 8D).

Digital Outcrop Model 3

The DOM (Fig. 9) is located near the southern edge of the study area, along the main road between Mânzălești and Lopătari (Fig. 6). It is west-east oriented with a length of 300 m and a height of 90 m (Fig. 9). The good exposure quality of the 3-D model enabled the extraction of 172 foliation measurements, with an average dip of 20° to the NW (Fig. 9D). We mapped multiple isoclinal folds of the foliation defined by different shades of grey banding (caused by varying amounts and types of inclusions), which are locally slightly anastomosing, forming tectonic lenses (Fig. 9A, D). The foliation is locally cross-cut by sub horizontal white bands (8° NE; Fig. 9A, B).

The inclusion-rich halite is locally exposed in outcrops at the base of the DOM, while in other parts it is covered by a precipitated layer of fine-grained porous halite that mimics the colour of the underlying salt. The exposed halite contains inclusions in a matrix of halite consisting of cm-size halite porphyroclasts surrounded by finer-grained halite (Figs. 5C, D, 10). The non-halite inclusions have a wide range in size and show no preferred orientation.

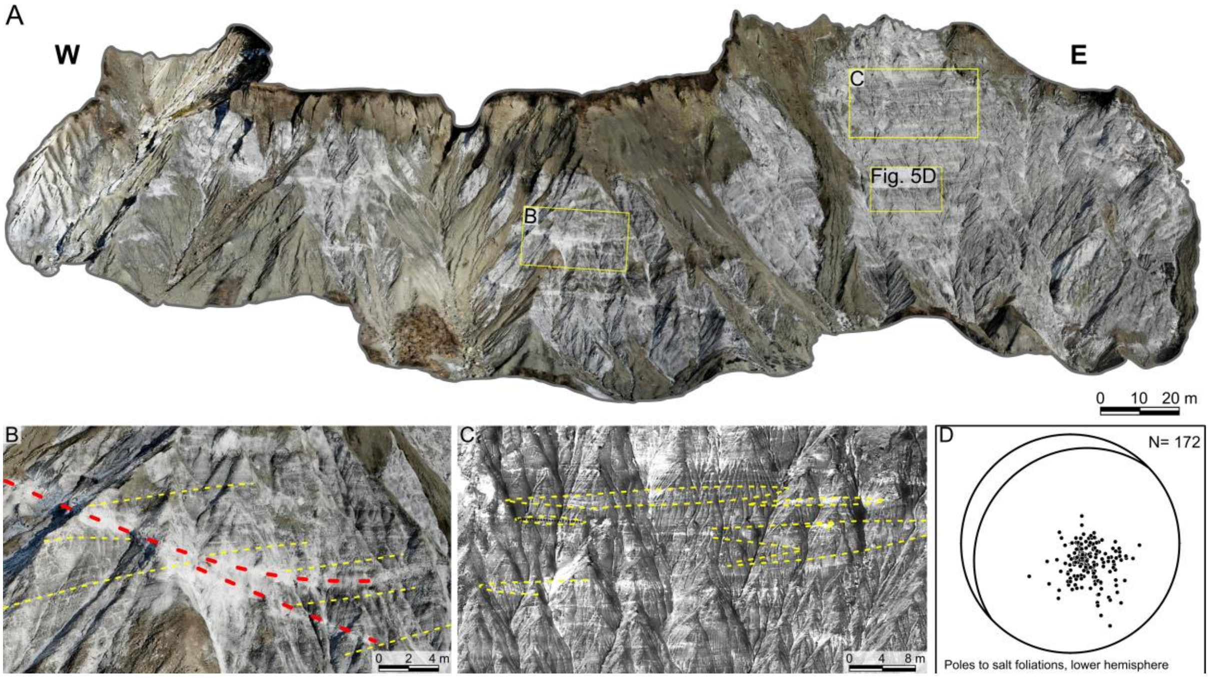

Figure 9. (A) Sideview of DOM 3, located in the SW of the Mânzălești salt diapir (with locations of Figs. 5D, 9B, C). (B) Detailed image extracted from the DOM illustrating the salt foliation (marked with yellow dashed lines; Fig. 9E) and the white bands cutting the foliation at a low angle (dashed red lines, see also Fig. 8B). (D) Detailed image extracted from the model illustrating isoclinal folding. (E) Lower-hemisphere stereonet plot showing poles to foliation (i.e. yellow dashed lines of Figs. 9B, C) and average orientation as a great circle.

Results of microstructural analysis

Microstructural analysis was performed on two samples (Fig. 10A, B) that are both rich in non-halite inclusions (14 wt %, Fig. 10A). Results show the inclusions are embedded in a halite matrix around the elongate halite porphyroclasts (Fig. 10C). XRD analysis of three particle classes in the insoluble residue shows beige sandstone, greenschist, and volcanic rock. Inclusions have a power-law distribution of grain sizes (Fig. 10B) and locally have fibrous strain shadows (Fig. 10D).

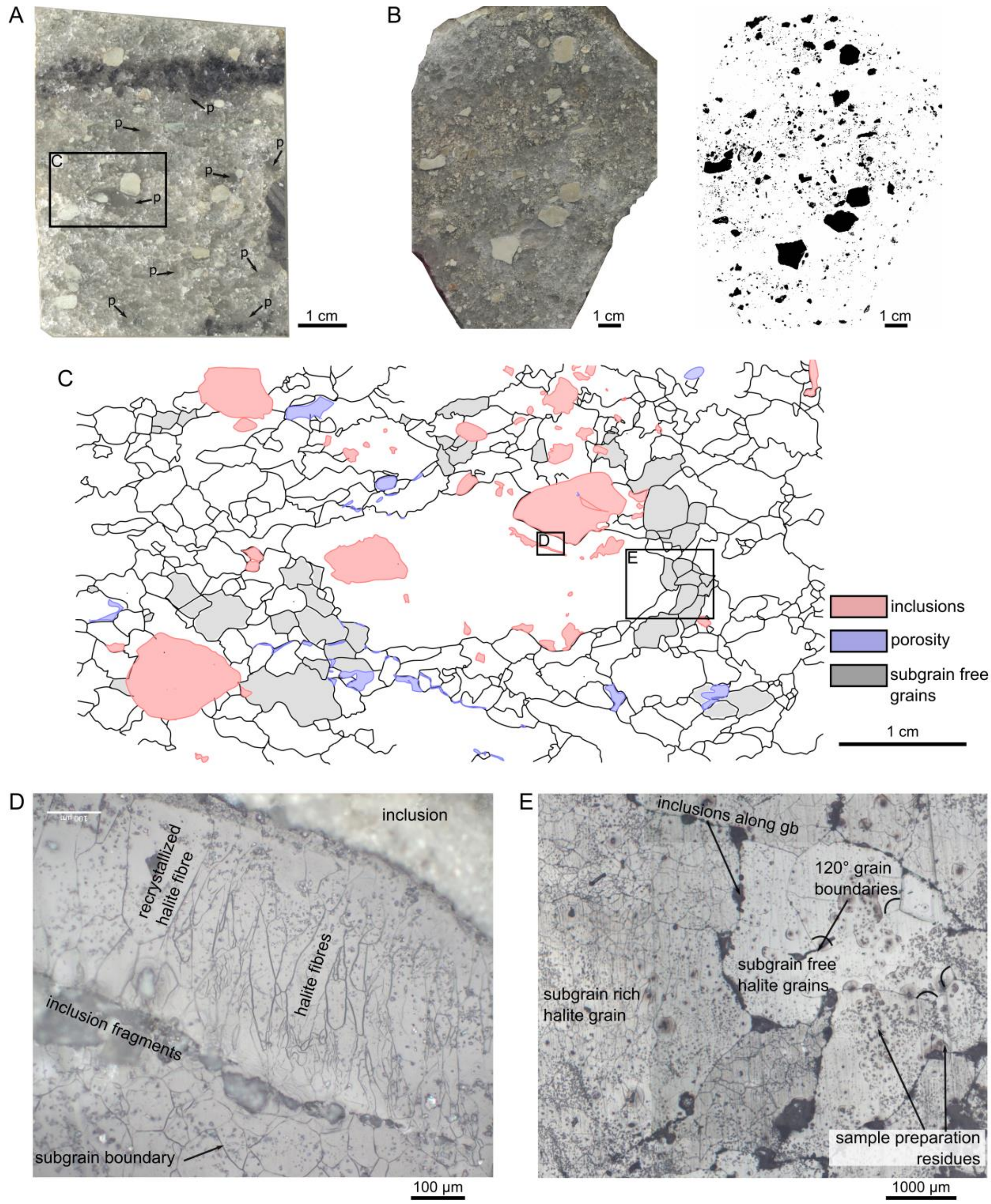

Figure 10. (A) Thin-section photograph of halite showing beige and black non-halite inclusions of variable grain sizes in a halite matrix with halite porphyroclasts (p) of up to 1 cm in diameter. (B) Halite sample (left) showing distribution of particles (right) that was used for grain-size analysis. (C) Map of traced halite grain boundaries, inclusions, and pores shows elongated and euhedral halite grains and large porphyroclast in the center; note

inclusion fragments inside the porphyroclast. (D) Halite fibres between fragmented non-halite inclusion. (E) Subgrains inside halite grain and subgrain-free halite grains with 120° grain boundaries and impurities along the boundaries. Small dark particles and brown halos (D, E) are due to etching residues on sample surface.

The halite matrix has a characteristic dynamically recrystallized microstructure with grains of about 1.5 mm, which are slightly elongated parallel to the foliation and have irregular, amoeboid shapes. Most halite grains (including the porphyroclasts) are rich in subgrains with an average size of 52 µm (n=520). Locally, halite grains are subgrain-free and have 120° grain boundaries (Fig. 10E). Using subgrain size piezometry (Schleder & Urai, 2005), this corresponds to a differential stress of 3.5 MPa. Recrystallized grainsize piezometry (Ter Heege et al., 2005) indicates a differential stress of about 4 MPa. High-angle grain boundaries in halite are rich in fluid inclusions and smaller non-halite particles are often present at grain boundaries and triple junctions. Halite fibres are only locally present in boudin necks between fragmented inclusions (Fig. 10D).

Cross-section

For constructing this profile (Fig. 11), we used the surface geology (stratigraphic boundaries, dip/azimuth of the layers, structural features), well and seismic data. The data show that the diapir is roughly 3,500 m tall and leans to the east. Flanking lower Miocene strata to the west are steeply dipping (82/245) in the proximity of the salt (Figs. 3B, 11). They are mostly concordant and stratigraphically conformable to the diapir edge and right-side-up. On the eastern flank, the contact of the salt with adjacent layers was not visible, being covered by the Quaternary deposits. Further away, however, lower Miocene layers are cropping out and are steeply dipping to the east. They become highly folded and thrusted, with mid-Miocene deposits in the hinges of small-scale synclines. This stratigraphy is buried to the east by the foreland deposits. Sub-salt, the layers are most likely characterised by duplexes as suggested by Schleder et al. (2019) and Tămaş at al. (2019).

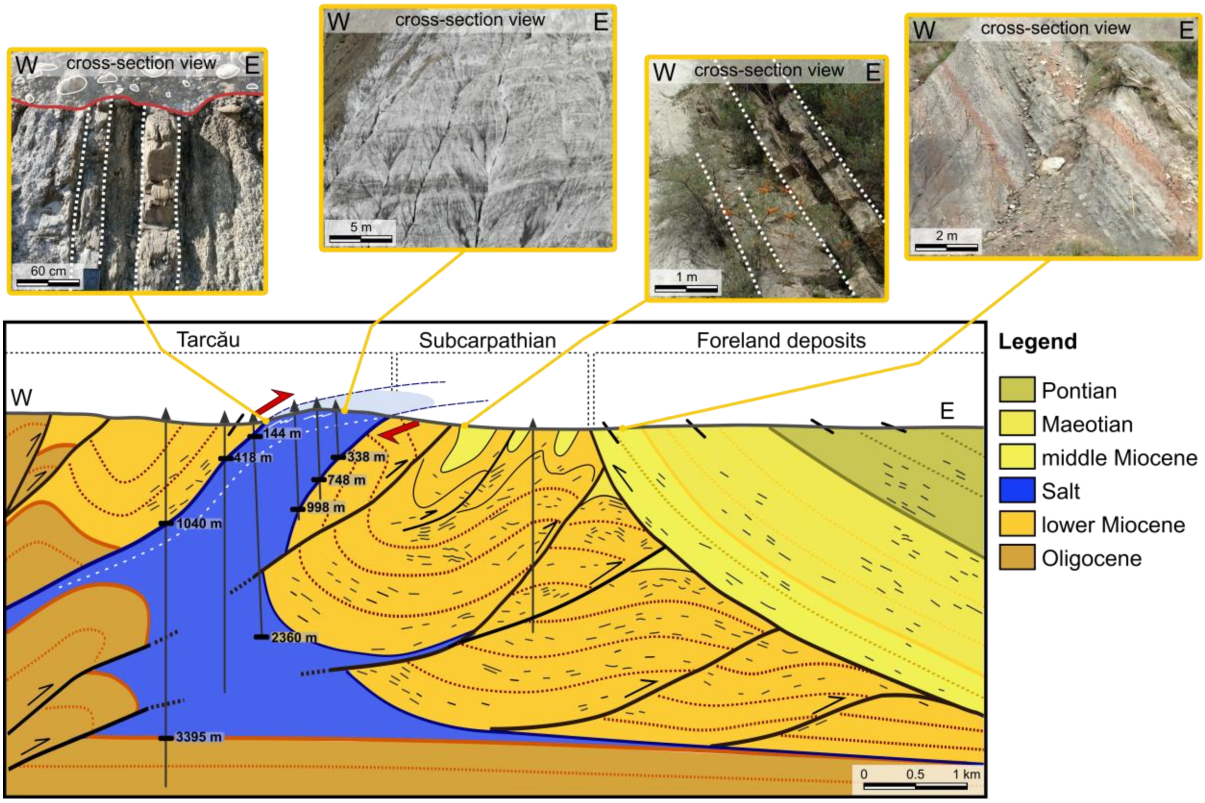

Figure 11. Cross-section through the Mânzălești diapir based on seismic and well data (Stoica & Gherasie, 1981; Marica, 2016), surface geology (Murgeanu et al., 1968), and structural styles from analogue modeling (Tămaș et al., 2019); location shown in Fig. 3. Inset photos show surface exposures.

The overall geometry, with concordant and conformable strata on the west but truncated strata at shallow levels to the east (Fig. 11), suggests that the diapir originated as an asymmetric salt-cored anticline that was breached by a thrust cutting the crestal part of the forelimb (in addition to deeper interpreted thrusts). In other words, it is an example of the asymmetric diapir folds identified by Mrazec (1910) in the Romanian Carpathians.

DISCUSSION

The Mânzălești diapir is the largest rock salt outcrop in Europe, described by many authors, but its structure was not clear, perhaps due to difficulties of access (unstable and dangerous, steep halite faces) and lack of microtectonic investigations. Using our high-resolution UAV-models and microstructural data allows for the first time a detailed structural analysis. In the discussion below, we consider four possible interpretations for the Mânzălești outcrop: (i) original subhorizontal layering of inclusion-rich depositional salt layers, (ii) eroded top of a long-lived passive diapir, (iii) salt glacier emplaced by lateral flow at the surface, and (iv) the sheared top of an incipient decapitated salt structure.

The origin of non-halite inclusions in some salt bodies in Romania has a long history of debate because they have aspects compatible with either sedimentary or tectonic melanges. Discrete layers of mixed halite and siliciclastics exist in the spectacular domal salt mine exposures in Romania (e.g., Ocnele Mari, Târgu Ocna, Slănic Prahova, Cacica), and in our samples, original halite porphyroclasts contain clastic inclusions. Both observations suggest a depositional origin, but the isoclinal folds together with the subhorizontal, gently anastamosing salt foliation in halite with large porphyroclasts surrounded by small recrystallized grains indicates intense subhorizontal shear overprinting any primary layering within the salt. Thus we reject hypothesis (i): in our interpretation the inclusions most likely formed as debris flows shed into the depositional evaporite basin during orogenic uplift (similar to what is observed in the Polish and Ukrainian Carpathians; Peryt & Kovalevich, 1997; Ślączka & Kolasa, 1997), with the consequent interbedded halite and non-halite layers subsequently sheared during the superimposed contractional deformation.

The fabric in the Mânzălești diapir contrasts strongly with the typical "domal" salt fabric observed in other Romanian diapirs. These are characterized by vertical to steeply-dipping, folded layers with larger, more equisized recrystallized grains deformed at lower differential stress. In our samples, microstructures show that halite was deformed by dislocation creep and water-assisted dynamic recrystallization under relatively high differential stresses of about 4 MPa, with solution-precipitation creep and fragmentation of the inclusions during deformation (see also Leitner et al., 2011). The large porphyroclasts are interpreted as the remnants of the original halite fabric (Schleder & Urai 2005, 2007; Závada et al., 2015). Thus, the subhorizontal fabric and high differential stress leads us to reject the interpretation in which the Mânzălești outcrop is the eroded top of a passive diapir.

Salt glaciers are characterized by fine-grained salt deformed at very low differential stress by dominantly solution-precipitation creep (Schleder & Urai, 2007; Desbois et al., 2010), with porphyroclasts rich in subgrains inherited from the rise of salt in the cold diapiric stem. Our microstructural observations (recrystallized grains contain abundant subgrains) and calculated differential stress levels are also incompatible with this, and thus we conclude that the surface outcrop at Mânzălești is not a salt glacier.

After combining observations at all scales (cross-sectional, outcrop, and microstructural analyses), our preferred explanation is that the Mânzălești diapir evolved from a salt-cored anticline into a thrusted diapir at the boundary between the Tarcău and Subcarpathian nappes. In effect, this is similar to the sketch in Figure 1D, but with the thrust cutting across the salt structure as in Figure 1C rather than emanating from within it. The relative foreland-directed movement of the Tarcău nappe, acccomodated elsewhere by the basal thrust, was accommodated in this location by intense shear within the upper portion of the original salt-cored anticline. Thus, the diapir is in the incipient stages of decapitation, shifting its upper, exposed portion somewhat away from its base. This happened at a shallow depth and fast strain rate to generate the relatively high differential stress during dominantly dislocation creep and water-assisted dynamic recrystallization with solution-deposition creep, but at sufficient depth to supress dilatancy (500 m is a reasonable estimate; see Urai et al., 2008).

Taking an average displacement rate on the frontal Tarcău thrust of 2 cm/year (Roure et al., 1993; Schleder et al., 2019) and a shear zone of 100 m thickness, the computed shear strain rate is $5x10^{-12}$ s^{-1}. Combining this with the independently obtained estimate of the differential stress of 4 MPa, we get an estimate of the rheology of the shear zone in reasonable agreement with the constitutive equation for halite rocks deforming by equal amounts of dislocation creep and solution-precipitation creep (cf. fig. 5.2.5 of Urai et al., 2008; ter Heege et al., 2005).

Finally, we interpret the near-horizontal surfaces of white salt, sometimes cross-cutting the salt foliation, as dilatant shear zones. These formed during deformation at low confining pressures close to the surface, with the colour modified by fluid flow (e.g., Urai et al., 2008; Davison, 2009). This presumably occurred during late uplift and erosional unroofing of the diapir during the latest stages of nappe advance.

CONCLUSIONS

We integrated UAV-based digital outcrop models, outcrop observations, microstructural analysis and subsurface data to get new insights into the Mânzălești diapir located in the Eastern Carpathians of Romania. The results of our study show:

- The extent of the salt at or just beneath the surface is about 2.7 km by 1.3 km wide, with about 200 m of relief. In the subsurface the diapir extends for about 3.5 km, demonstrating a deep-rooted salt body.
- Many sinkholes have been identified, especially in the south-western area. It is also covered by small lakes, most likely associated with sinkholes.
- In outcrop, especially in steep faces, the halite is locally exposed and presents solution grooves (rillenkarren), while in other parts it is covered by a precipitated layer of fine-grained porous halite that mimics the colour of the underlying salt.

- UAV-based digital outcrop models enabled the measurement of generally low-dipping (20-34°) salt foliation, with a higher average in the SW edge of the salt dome (53°). Isoclinal folds and low-dipping shear zones have also been identified.
- The exposed salt has a high amount of impurities, ranging from mm to m-scale blocks of various lithologies (sandstones, limestones, green schists, volcanics).
- The impurities are hosted in a matrix of halite consisting of cm-size porphyroclasts surrounded by finer-grained halite.
- Microstructures show that halite was deformed by dislocation creep and water-assisted dynamic recrystallization under relatively high differential stresses of about 4 MPa, with solution-precipitation creep and fragmentation of the non-halite inclusions during deformation.

We interpret the Mânzălești salt diapir to have evolved from a salt-cored anticline into a thrusted diapir in front of the Tarcău nappe. Foreland-directed movement of the nappe sheared the top of the diapir, leading to incipient decapitation. The deformation we see in the outcrop happened at a shallow depth and fast strain rates, as demonstrated by the microstructural analysis.

ACKNOWLEDGEMENTS

Pleșa Adrian, Relu D. Roban and Dan Jipa are thanked for insightful discussions, and the latter shared one of the halite samples. XRD analysis was performed by Nicolai Thüns. Schlumberger and M. El Toukhy kindly provided the seismic data in Fig. 1A; this seismic data is proprietary and can be only shown in the figure. Other used seismic and well data is available through Stoica and Gherasie, 1981 and Marica, 2016. Digital outcrop models 1-3 as well as the DEM will be made available as .obj models on pangaea.de.

REFERENCES

Aftabi, P., Roustaie, M., Alsop, G. I., & Talbot, C. J. (2010). InSAR mapping and modelling of an active Iranian salt extrusion. *Journal of the Geological Society*, 167, 155–170. https://doi.org/10.1144/0016-76492008-165

Allmendinger, R. W., Cardozo, N. C., & Fisher, D. (2013). *Structural Geology Algorithms: Vectors & Tensors*. Cambridge, UK: Cambridge University Press.

Athanasiu, S. (1916). Discuționea asupra vârstei formațiunei salifere din România. *Dări de Seamă, Institutul Geologic al României*, 5, 22–32.

Bahrami, S., Capolongo, D., & Mofrad, M. R. (2020). Morphometry of drainage basins and stream networks as an indicator of active fold growth (Gorm anticline, Fars Province, Iran). *Geomorphology*, 355, 107086. https://doi.org/10.1016/j.geomorph.2020.107086

Băncilă, I. (1958). *Geologia Carpaților Orientali*. Bucharest, Romania: Editura Tehnică.

Barnhart, W. D., & Lohman, R. B. (2012). Regional trends in active diapirism revealed by mountain range-scale InSAR time series: Active Zagros Diapirism. *Geophysical Research Letters*, 39(8). https://doi.org/10.1029/2012GL051255

Beloussov, V. V. (1959). Types of folding and their origin. *International Geology Review*, 1(2), 1-21. https://doi.org/10.1080/00206815909473393

Burliga, S., Krzywiec, P., Dąbroś, K., Przybyło, J., Włodarczyk, E., Źróbek, M., & Słotwiński, M. (2018). Salt tectonics in front of the Outer Carpathian thrust wedge in the Wieliczka area (S Poland) and its exposure in the underground salt mine. *Geology, Geophysics & Environment*, 44(1), 71. https://doi.org/10.7494/geol.2018.44.1.71

Callot, J.-P., Jahani, S., & Letouzey, J. (2007). The role of pre-existing diapirs in fold and thrust best development. In O. Lacombe, F. Roure, J. Lavé, J. Vergés, (Eds.), *Thrust Belts and Foreland Basins* (pp. 309-325). Berlin: Springer. https://doi.org/10.1007/978-3-540-69426-7_16

Cardozo, N., & Allmendinger, R. W. (2013) Spherical projections with OSXStereonet: *Computers & Geosciences*, 51, 193-205. https://doi.org/10.1016/j.cageo.2012.07.021

Cobălcescu, G. (1883). Studii geologice și paleontologice asupra unor tĕràmuri terțiare din unile părți ale Romăniei: Memoriile Geologice ale Scolei Militare din Iasi. Bucharest, Romania: Stabilimentul grafic Socecu & Teclu.

Coward, M. P., & Stewart, S. (1995). Salt-influenced structures in the Mesozoic-Tertiary cover of the southern North Sea, U.K. In M. P. A. Jackson, D. G. Roberts, S. Snelson (Eds.), *Salt tectonics: a global perspective* (AAPG Memoir 65, pp. 229-250), AAPG. https://doi.org/10.1306/M65604C10

Csontos, L. & Vörös, A. (2004). Mesozoic plate tectonic reconstruction of the Carpathian region. *Palaeogeography, Palaeoclimatology, Palaeoecology*, 210, 1–56. https://doi.org/10.1016/j.palaeo.2004.02.033

Davis, D. M., & Engelder, T. (1985). The role of salt in fold-and-thrust belts. *Tectonophysics*, 119, 67-88. https://doi.org/10.1016/0040-1951(85)90033-2

Davison, I. (2009). Faulting and fluid flow through salt. *Journal of the Geological Society*, 166(2), 205–216. https://doi.org/10.1144/0016-76492008-064

Desbois, G., Závada, P., Schleder, Z., & Urai, J. L. (2010) Deformation and recrystallization mechanisms in actively extruding salt fountain: Microstructural evidence for a switch in deformation mechanisms with increased availability of meteoric water and decreased grain size (Qum Kuh, Central Iran). *Journal of Structural Geology*, 32(4), 580-594. https://doi.org/10.1016/j.jsg.2010.03.005

Duffy, O. B., Dooley, T. P., Hudec, M. R., Jackson, M. P. A., Fernandez, N., Jackson, C. A.-L., & Soto, J. I. (2018). Structural evolution of salt-influenced fold-and-thrust belts: a synthesis and new insights from basins containing isolated salt diapirs. *Journal of Structural Geology*, 114, 206-221. https://doi.org/10.1016/j.jsg.2018.06.024

Dumitrescu, I. (1948). La Nappe du Gres de Tarcău, la zone marginale et la zone neogene, entre Casin et Putna: Comptes Rendus deo Seances. *Institut Geologique de Roumanie*, 29, 84–105.

Dumitrescu, I. (1952). Etude Geologique de la region entre l'Oituz et la Coza. *Anuarul Institutului Geologic al Romaniei*, 14, 195–218.

Dumitrescu, I., Săndulescu, M., & Bandrabur, T. (1970). *Geological Map of Romania (sheet 29-Covasna, scale 1:200000)*. Bucharest, Romania: Geological Institute of Romania, explanatory text, 80 p.

Ferrer, J. O. (2012). Salt Tectonics in the Parentis Basin (Eastern Bay of Biscay): Origin and Kinematics of Salt Structures in a Hyperextended Margin Affected by Subsequent Contractional Deformation (Doctoral dissertation). Barcelona, Spain, University of Barcelona.

Filipescu, S., Tămaș D. M., Bercea R., Tămaș A., Bălc, R., Țabără, D., et al. (2020). The biostratigraphic reevaluation of the lower to middle Miocene formations from the Eastern Carpathians: a case study related to the oil fields of the Diapir Fold Zone, Romania. *Geological Quarterly*, 64(3), 781–800. https://doi.org/10.7306/gq.1554

Giurgiu, I. (2010). Cea mai mare peșteră în sare din România. *Natura României*, 3, 1-234.

Gutiérrez, F., & Lizaga, I. (2016). Sinkholes, collapse structures and large landslides in an active salt dome submerged by a reservoir: The unique case of the Ambal ridge in the Karun River, Zagros Mountains, Iran. *Geomorphology*, 254, 88–103. https://doi.org/10.1016/j.geomorph.2015.11.020

Gutiérrez, F., Sevil, J., Silva, P. G., Roca, E., & Escosa, F. (2019). Geomorphic and stratigraphic evidence of Quaternary diapiric activity enhanced by fluvial incision. Navarrés salt wall and graben system, SE Spain. *Geomorphology*, 342, 176–195. https://doi.org/10.1016/j.geomorph.2019.06.002

Hodgetts, D. (2010). Collection, processing, interpretation and modelling of digital outcrop data using VRGS: An integrated approach to outcrop modelling. Paper presented at 72nd EAGE Conference and Exhibition-Workshops and Fieldtrips (pp. cp-162).

Hudec, M. R., & Jackson, M. P. A. (2007). Terra infirma: understanding salt tectonics. *Earth-Science Reviews*, 82, 1-28. https://doi.org/10.1016/j.earscirev.2007.01.001.

Jackson, M. P. A., & Hudec, M. R. (2017). *Salt Tectonics – Principles and Practice*. Cambridge, UK: Cambridge University Press. https://doi.org/10.1017/9781139003988

Jahani, S., Callot, J.-P., de Lamotte, D. F., Letouzey, J., & Leturmy, P. (2007). The Salt Diapirs of the Eastern Fars Province (Zagros, Iran): A Brief Outline of their Past and Present. In O. Lacombe, F. Roure, J. Lavé, J. Vergés, (Eds.), *Thrust Belts and Foreland Basins* (pp. 289-308). Berlin: Springer. https://doi.org/10.1007/978-3-540-69426-7_15

Lazarev, S., de Leeuw, A., Stoica, M., Mandic, O., van Baak, C. G. C., Vasiliev, I., & Krijgsman, W. (2020). From Khersonian drying to Pontian flooding: late Miocene stratigraphy and palaeoenvironmental evolution of the Dacian Basin (Eastern Paratethys). *Global and Planetary Change*, 192, 103224. https://doi.org/10.1016/j.gloplacha.2020.103224

Leitner, C., Neubauer, F., Urai, J. L., & Schoenherr, J. (2011). Structure and evolution of a rocksalt-mudrock-tectonite: The Haselgebirge in the Northern Calcareous Alps. *Journal of Structural Geology*, 33(5), 970-984. https://doi.org/10.1016/j.jsg.2011.02.008

Letouzey, J., Colletta, B., Vially, R., & Chermette, J. C. (1995). Evolution of salt-related structures in compressional settings. In M. P. A. Jackson, D. G. Roberts, S. Snelson (Eds.), *Salt tectonics: a global perspective* (AAPG Memoir 65, pp. 41-60), AAPG. https://doi.org/10.1306/M65604C3

Marica, I. S. (2016). Aplicaţii ale măsurătorilor geofizice în studiul masivelor de sare din România - Zona Cutelor Diapire (Doctoral dissertation). Bucharest, Romania, Bucharest University.

Mațenco, L., & Bertotti, G. (2000). Tertiary tectonic evolution of the external East Carpathians (Romania). *Tectonophysics*, 316, 255–286. https://doi.org/10.1016/S0040-1951(99)00261-9

Mațenco, L. (2017). Tectonics and exhumation of the Romanian Carpathians: Inferences from kinematic and thermochronological studies. In M. Radoane, A. Vespremeanu-Stroe (Eds.), *Landform Dynamics and Evolution in Romania* (pp. 15-56), Springer Geography. https://doi.org/10.1007/978-3-319-32589-7_2

Melinte-Dobrinescu, M. C., Brustur, T., Jipa, D., Macaleţ, R., Ion, G., Ion, E., et al. (2017). The Geological and Palaeontological Heritage of the Buzău Land Geopark (Carpathians, Romania). *Geoheritage*, 9, 225–236. https://doi.org/10.1007/s12371-016-0202-3

Meruțiu, V. (1912). *Contribuțiune la studiul masivelor de sare din România*. Bucharest, Romania: Stabilimentul de arte grafice Albert Baer.

Mrazec, L. (1910). Über die Bildung der rumänischen Petroleumlagerstätten. *Third International Petroleum Conference: Compte Rendu*, 2, 80-134.

Mrazec, L., & Teisseyre, W. (1902). Privire geologică asupra formaţiunilor salifere şi zăcămintelor de sare din România. *Monitorul Petrolului Român*, 3, 1–55.

Mrazec, L. & Voitești, I. P. (1914). Contributions a la connaissance des nappes du Flysch Carpatique en Roumanie. *Anuarul Institutului Geologic al Romaniei*, 5, 495–527.

Murgeanu, G., Dumitrescu, I., Săndulescu, M., Bandrabur, T., & Săndulescu, J. (1968) *Geological Map of Romania (sheet 29-Covasna, scale 1:200000)*. Bucharest, Romania: Geological Institute of Romania.

Olteanu, F. (1951). Observații asupra 'breciei sării', cu masive de sare din regiunea mio-pliocenă dintre R. Teleajenului și P. Bălăneasa (cu privire specială pentru regiunea Pietraru-Buzău). *Dări de Seamă, Institutul geologic al României*, 32, 12-18.

Peryt, T. M., & Kovalevich, V. M. (1997). Association of redeposited salt breccias and potash evaporites in the Lower Miocene of Stebnyk (Carpathian foredeep, West Ukraine): *Journal of Sedimentary Research*, 67, 913–922. https://doi.org/10.1306/D4268676-2B26-11D7-8648000102C1865D

Pichel, L. M., Finch, E., Huuse, M., & Redfern, J. (2017). The influence of shortening and sedimentation on rejuvanation of salt diapirs: a new discrete-element modelling approach. *Journal of Structural Geology*, 104, 61-79. https://doi.org/10.1016/j.jsg.2017.09.016

Ponta, G. M. L. (2019). Eastern Subcarpathians Bend: Salt Karst: Meledic Plateau and Slănic Prahova. In G. M. L. Ponta, B. P. Onac (Eds.), *Cave and Karst Systems of Romania, Cave and Karst Systems of the World* (pp. 451–454), Springer International Publishing. https://doi.org/10.1007/978-3-319-90747-5_51

Popescu, G. (1951). Observațiuni asupra ‘breciei sării’ și a unor masive de sare din zona paleogenă-miocenă a jud. Prahova. *Dări de Seama, Institutul geologic al României*, 32, 3-12.

QGIS Development Team (2020). *QGIS Geographic Information System*. Open Source Geospatial Foundation Project. http://qgis.osgeo.org

Roosta, H., Jalalifar, H., Karimi Nasab, S., & Ranjbar, M. (2019). Surface deformation over the buried Nasr Abad salt diapir, Central Iran using interferometric synthetic aperture radar data. *International Journal of Remote Sensing*, 40, 8322–8341. https://doi.org/10.1080/01431161.2019.1608386

Roure, F., Roca, E., & Sassi, W. (1993). The Neogene evolution of the outer Carpathian flysch units (Poland, Ukraine and Romania): kinematics of a foreland/fold-and-thrust belt system. *Sedimentary Geology*, 86, 177–201. https://doi.org/10.1016/0037-0738(93)90139-V

Rowan, M. G., & Vendeville, B. C. (2006). Foldbelts with early salt withdrawal and diapirism: physical model and examples from the northern Gulf of Mexico and the Flinders

Ranges, Australia. *Marine and Petroleum Geology*, 23, 871-891. https://doi.org/10.1016/j.marpetgeo.2006.08.003

Săndulescu, M. (1984). *Geotectonica României*. Bucharest, Romania: Editura Tehnică.

Săndulescu, M. (1988). Cenozoic Tectonic History of the Carpathians. In: L. H. Royden, F. Horváth (Eds.), *The Pannonian Basin: A Study in Basin Evolution* (AAPG Memoir 45, pp. 17–25), AAPG. https://doi.org/10.1306/M45474C2

Sarkarinejad, K., Sarshar, M. A., & Adineh, S. (2018). Structural, micro-structural and kinematic analyses of channel flow in the Karmostaj salt diapir in the Zagros foreland folded belt, Fars province, Iran. *Journal of Structural Geology*, 107, 109–131. https://doi.org/10.1016/j.jsg.2017.12.005

Sasvári, Á., & Baharev, A. (2014). SG2PS (structural geology to postscript converter)–A graphical solution for brittle structural data evaluation and paleostress calculation. *Computers & Geosciences*, 66, 81-93. https://doi.org/10.1016/j.cageo.2013.12.010

Schindelin, J., Arganda-Carreras, I., Frise, E., Kaynig, V., Longair, M., Pietzsch T., et al. (2012). Fiji: an open-source platform for biological-image analysis. *Nature methods*, 9(7), 676-682. https://doi.org/10.1038/nmeth.2019

Schleder, Z., & Urai, J. L. (2005). Microstructural evolution of deformation- modified primary Halite from Hengelo, the Netherlands. *International Journal of Earth Sciences (Geol Rundsch)*, 94(5-6), 941-956. https://doi.org/10.1007/s00531-005-0503-2

Schleder, Z., & Urai, J. L. (2007). Deformation and recrystallization mechanisms in Mylonitic shear zones in naturally deformed extrusive Eocene-Oligocene rocksalt from Eyvanekey Plateau and Garmsar Hills (Central Iran). *Journal of Structural Geology*, 29(2), 241-255. https://doi.org/10.1016/j.jsg.2006.08.014

Schleder, Z., Tămaș, D. M., Krézsek, C., Arnberger, K., & Tulucan, A. (2019). Salt tectonics in the Bend Zone segment of the Carpathian fold and thrust belt, Romania: *International*

Journal of Earth Sciences (Geol Rundsch), 108, 1595–1614. https://doi.org/10.1007/s00531-019-01721-x

Schmid, S. M., Bernoulli, D., Fügenschuh, B., Mațenco, L., Schefer, S., Schuster, R., et al. (2008). The Alpine-Carpathian-Dinaridic orogenic system: correlation and evolution of tectonic units. *Swiss Journal of Geosciences*, 101, 139–183. https://doi.org/10.1007/s00015-008-1247-3

Schorn, A., & Neubauer, F. (2014). The structure of the Hallstatt evaporite body (Northern Calcareous Alps, Austria): A compressive diapir superposed by strike-slip shear?. *Journal of Structural Geology*, 60, 70–84. https://doi.org/10.1016/j.jsg.2013.12.008

Ślączka, A., & Kolasa, K. (1997) Resedimented salt in the Northern Carpathians Foredeep (Wieliczka, Poland). *Slovak Geological Magazine*, 3, 135-155.

Snidero, M., Muñoz, J.A., Carrera, N., Butillé, M., Mencos, J., Motamedi, H., et al. (2019). Temporal evolution of the Darmadan salt diapir, eastern Fars region, Iran. *Tectonophysics*, 766, 115-130. https://doi.org/10.1016/j.tecto.2019.06.006

Spruzeniece, L., Schmatz, J., Virgo, S., & Urai, J. L. (2019). Virtual microscopy for geosciences. *EGU blog: Minds over Methods*. Source: https://blogs.egu.eu/divisions/ts/2019/07/23/virtual-microscopy-for-geosciences/

Stoica, C., & Gherasie, I. (1981). *Sarea și sărurile de potasiu și magneziu din România*. Craiova, Romania: Intreprinderea poligrafica "Oltenia".

Talbot, C. J. (1998). Extrusions of Hormuz salt in Iran. *Geological Society, London, Special Publications*, 143, 315–334. https://doi.org/10.1144/GSL.SP.1998.143.01.21

Talbot, C. J., & Rogers, E. A. (1980). Seasonal Movements in a Salt Glacier in Iran. *Science*, 208, 395–397. https://doi.org/10.1126/science.208.4442.395

Tămaş, D. M., Schleder, Z., Krézsek, C., Man, S., & Filipescu, S. (2018). Understanding salt in orogenic settings: The evolution of ideas in the Romanian Carpathians. *AAPG Bulletin*, 102, 941–958. https://doi.org/10.1306/0913171615517088

Tămaș, D. M., Schleder, Z., Tămaș, A., Krézsek, C., Copoț, B., & Filipescu, S. (2019). Middle Miocene evolution and structural style of the Diapir Fold Zone, Eastern Carpathian Bend Zone, Romania: insights from scaled analogue modelling. In J. Hammerstein, R. Di Cuia, P. Griffiths, M. Cottam, G. Zamora, R. Butler (Eds.), *Fold and Thrust Belts: Structural Style, Evolution and Exploration* (Special Publications 490, pp. 267-284). Geological Society of London. https://doi.org/10.1144/SP490-2019-091

Ter Heege, J. H., De Bresser, J. H. P., & Spiers, C.J. (2005). Dynamic recrystallization of wet synthetic polycrystalline halite: dependence of grain size distribution on flow stress, temperature and strain. *Tectonophysics*, 396, 35–57. https://doi.org/10.1016/j.tecto.2004.10.002

Urai, J. L., Schleder, Z., Spiers, C. J., & Kukla, P. A. (2008). Flow and Transport Properties of Salt Rocks. In R. Littke, U. Bayer, D. Gajewski, S. Nelskamp (Eds.), *Dynamics of Complex Intracontinental Basins: The Central European Basin System* (pp. 277-290). Springer-Verlag, Berlin. https://doi.org/10.1007/978-3-540-85085-4_5

Urai, J. L., Spiers, C. J., Peach, C. J., Franssen, R. C. M. W., & Liezenberg, J. L. (1987). Deformation mechanisms operating in naturally deformed halite rocks as deduced from microstructural investigations. *Geologie en Mijnbouw*, 66: 165-176.

Urecheatu, M. M., Tămaș, D. M., & Roban, R. D. (2019). *De la fotogrametrie 3D si modelare analogică la evoluția cinematică a diapirului de la Mânzălești*. Paper presented at National Geology and Geophysics Student Conference, Edition XX, Bucharest, Romania.

Voitești, I. P. (1943). *Sarea regiunilor carpatice Românești.* Bucharest, Romania: Fundația Regală pentru literatură și artă.

Weismüller, C., Urai, J. L., Kettermann, M., von Hagke, C., & Reicherter, K. (2019). Structure of massively dilatant faults in Iceland: lessons learned from high-resolution unmanned aerial vehicle data. *Solid Earth*, 10, 1757–1784. https://doi.org/10.5194/se-10-1757-2019

Závada, P., Desbois, G., Urai, J. L., Schulmann, K., Rahmati, M., & Lexa, O. (2015). Impact of solid second phases on deformation mechanisms of naturally deformed salt rocks (Kuh-e-Namak, Dashti, Iran) and rheological stratification of the Hormuz Salt Formation. *Journal of Structural Geology*, 74, 117–144. https://doi.org/10.1016/j.jsg.2015.02.009

Zucker, E., Frumkin, A., Agnon, A., & Weinberger, R. (2019). Internal deformation and uplift-rate of salt walls detected by a displaced dissolution surface, Dead Sea basin. *Journal of Structural Geology*, 127, 103870. https://doi.org/10.1016/j.jsg.2019.103870